
Article:
Ferreira, FPV, Tsavdaridis, KD orcid.org/0000-0001-8349-3979, Martins, CH et al. (1 more author) (2021) Buckling and Post-Buckling Analyses of Composite Cellular Beams. Composite Structures, 262. 113616. ISSN 0263-8223

https://doi.org/10.1016/j.compstruct.2021.113616

Buckling and post-buckling analyses of composite cellular beams

Felipe Piana Vendramell Ferreira*[a], Konstantinos Daniel Tsavdaridis[b], Carlos Humberto Martins[c], Silvana De Nardin[a]

[a]Department of Civil Engineering, Federal University of São Carlos, Rod. Washington Luiz, km 235, São Carlos, São Paulo, Brazil.

[b]School of Civil Engineering, Faculty of Engineering and Physical Sciences, University of Leeds, Woodhouse Lane, LS2 9JT Leeds, UK.

[c]Department of Civil Engineering, State University of Maringá, Av. Colombo nº 5790, Maringá, Paraná, Brazil.

*Corresponding author

E-mail address: fpiana@live.com (F. P. V. Ferreira), K.Tsavdaridis@leeds.ac.uk (K. D. Tsavdaridis), chmartins@uem.br (C. H. Martins), snardin@ufscar.br (S. De Nardin)

Abstract

This paper aims to investigate the buckling and post-buckling analyses of composite cellular beams. For this, the numerical model is calibrated by experimental tests via post-buckling analysis. A parametric study is developed, considering six cross sections. For each section, the opening diameter and web post length are varied. Regarding the buckling analyses for the symmetrical sections, it was concluded that the end post is an important parameter in the strength of composite cellular beams that presents high web slenderness. The smaller the opening diameter, the greater the critical global shear. The variation in the height of the cellular beam had a little influence on larger diameters and web posts widths. Considering asymmetric sections, it was verified that the web post buckling did not happen for the first buckling mode. In this scenario, local web buckling of the upper tee was observed. With the height variation, there was an increase in the global shear. This is due to the fact that with the increase in height, the buckling mode was transferred to the WPB, instead of local web buckling. Finally, there was a conservatism in the SCI P355 calculation recommendations, a factor that needs to be revised.

Keywords: Composite cellular beams; Critical global shear; Finite element analysis; Buckling; Post-buckling.

NOTATION

The following symbols are used in this paper:

b	the width of the concrete slab	l_{eff}	effective length of web-post
b_f	the width of the flange	V	the global shear
b_w	the width of the web post	V_{cr}	the critical global shear
b_{we}	the width of the end post	L_b	the unrestrained length of composite cellular beam
D_o	the opening diameter	L_p	the distance between support and load
E	Young's modulus	p	the length between the opening diameter centers
d	the depth of parent section;	t_f	the thickness of the flange
d_g	the depth of cellular beam	t_w	the thickness of the web
f_c	the compressive cylinder strength of concrete	α	the imperfection factor
$f_{cr,w}$	the critical stress at web post	λ_w	the web slenderness ratio
f_t	the concrete tension resistance	$\overline{\lambda}$	the reduced slenderness factor
f_u	the ultimate strength of cellular beam	χ	the reduction factor
f_y	the yield strength of cellular beam		

1. INTRODUCTION

Cellular beams are those with circular sequential openings along the web, manufactured from thermal cutting and welding, aiming at the expansion of the cross section. Such beams are used in the design of parking garages, industries and warehouses, factories, office buildings, schools, hospitals and offshore elements. The presence of the openings influences the air flow, as well as the integration of services through ducts. However, due to the presence of openings, cellular beams are more susceptible to buckling modes, such as lateral torsional buckling, web distortion, web post buckling (WPB) or even the combination of the buckling modes [1–3], although the formation of the plastic mechanism, such as the Vierendeel mechanism (VM), can also occur. In the case of composite cellular beams, due to the compressed cellular beam flange being restrained by the concrete slab, the ultimate strength of these structures occur through the association of the failure mechanisms of the cellular beams, in this case VM or WPB, with the mechanisms of the concrete slab, i.e. cracking or crushing [4–8]. VM occurs when the tees reach the yield strength, caused by the combination of normal and tangential stresses. This phenomenon is characterized by the formation of plastic hinges near to the opening [9]. The main parameters that affect this structural behavior are the web thickness and the depth of tee [10–12]. On the other hand, the WPB is characterized by a double curvature, in the shape of an "S", which occurs in the web post according to the geometric characteristics of the cellular profile, such as opening diameter, the web post width and the web thickness [13].

In Abrambes et al. [14] the elastic buckling analyses of non-composite cellular beams were estimated using an artificial neural network (ANN). In this study, the authors found that WPB occurred for sections with slender web posts. In Rajana et al. [15] elastic and inelastic analyses were presented in non-composite cellular beams, the purpose of which was to illustrate the influence

of geometric parameters on the resistance of these structural elements based on the requirements of SCI P355 [15]. Such a study is the motivation for carrying out analyses on composite cellular beams. With a focus on WPB, the SCI P355 [15] recommendations address a truss model for calculating resistance. In this model, which is based on the EC3 [16], it starts by elastic analysis, and then the buckling curves are associated (**Fig. 1**). Regarding the selection of the buckling curves, for the case of double symmetrical hot-rolled sections, the buckling curves *a*, *b* and *c* can be used in the design of sections that have d/b_f>1.2. In this context, for sections with t_f≤40mm, the buckling curves *a* and *b* are used when the buckling occurs around the strong and weak axes, respectively. For hot-rolled sections that have d/b_f≤1.2 and 40mm≤t_f ≤100mm, the buckling curves *b* and *c* are recommended for the occurrence of buckling around the strong and weak axes, respectively. On the other hand, for doubly symmetrical welded sections, the classification of the use of buckling curves is limited only in the flange thickness. For sections with t_f≤40mm, buckling curves *b* and *c* are recommended for the occurrence of buckling around strong and weak axes, respectively. For t_f>40mm, buckling curves *c* and *d* are recommended, depending on the strong and weak axes. In the case of cellular beams, it is recommended to use the buckling curves *b* and *c* for hot-rolled and welded sections, respectively, considering the web post buckling. **Table 1** shows the imperfection factor (α) values for each buckling curve.

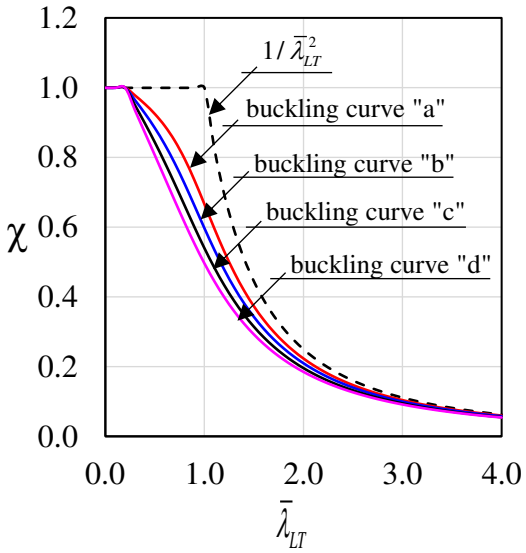

Fig. 1: EC3 buckling curves

Table 1: Imperfection factors for buckling curves according EC3

Buckling curve	*a*	*b*	*c*	*d*
Imperfection factor (α)	0.21	0.34	0.49	0.76

The paper aims to investigate numerically elastic analyses in composite cellular beams. The finite element model is calibrated, considering tests via inelastic analyses. The model is represented, considering the structural system of composite cellular beams formed by cellular beams, headed stud connectors and composite slabs (with Holorib HR 51/150 geometry). Subsequently, a parametric study is developed, varying the key parameters such as the opening diameter and web post width. In this study, six

geometric sections are considered, that is, three symmetric sections and three asymmetric sections. In total, 120 elastic analyses are performed. The results are presented and discussed, considering the buckling modes and the critical global shear that causes WPB. Also, the results are compared with the inelastic analyses, previously presented in Ferreira et al. [17], and with the calculation of the critical global shear presented in [13,18].

2. BACKGROUND

There are studies on composite beams with only a rectangular web opening, considering solid [19–26] or composite slabs [4,5,32–34,6,7,11,27–31]. The present paper focuses on studies of composite cellular beams, which are recent; mainly those initiated in the 2000s. In this scenario, there are several experimental and numerical investigations that evaluated the behavior of composite cellular beams [8,17,35–39]. Hechler et al. [35] and Müller et al. [36] presented test from two models: composite symmetric and asymmetric cellular beams. Both specimens were designed in such a way that at one end it was possible to investigate the composite action, at the other end, only the cellular beam. According to the authors, the VM was observed for low loading values at the end corresponding to the composite cellular beam. However, at the end where there was only the cellular steel profile, the strength was reached by WPB. In the same way, Nadjai et al. [37] presented tests results of composite symmetric and asymmetric cellular beams. Both models had the strength governed by WPB. Gizejowski and Khalil [39] performed a set of tests on composite cellular beams subjected to negative bending moment. In all situations, the authors observed failure modes associated with web distortion. Sheehan et al. [8] tested composite asymmetric cellular beams, situation in which the lower tee consists of a section heavier than the upper tee, with large spans. The authors observed that the composite cellular beam requested for uniformly distributed loads resisted 3.4 times the estimated design load, despite the degree of interaction considerably less than the minimum required by EC4 [40]. In Ferreira et al. [17] the resistance of steel-concrete composite cellular beams was investigated by inelastic analyses. In this study it was found that the procedures for calculating WPB are conservative [13,18,41,42]. Although there are several analytical calculation models in the literature, considering the WPB, as presented in Ferreira et al. [43], the present study focuses on the SCI P355 procedure [17,42]. Such a model is based on strut, considering the effective length, which takes into account the variation of stresses around the opening, according to **Eq. (1)**. Once the effective length has been determined, then the theory of compression bars, according to EN 1993-1-1 [44], is applied, considering slenderness in the web post length and using the buckling curve *b* and *c* (**Fig. 1**) for hot-rolled and welding members, respectively (**Eqs. 2-8**):

$$l_{eff} = 0.5\sqrt{b_w^2 + D_o^2} \le 0.7D_o \tag{1}$$

$$\sigma_{Rk} = \chi f_y \tag{2}$$

$$\chi = \frac{1}{\phi + \sqrt{\phi^2 - \bar{\lambda}^2}} \le 1.0 \tag{3}$$

$$\phi = 0.5\left[1 + \alpha\left(\bar{\lambda} - 0.2\right) + \bar{\lambda}^2\right] \tag{4}$$

$$\bar{\lambda} = \sqrt{\frac{f_y}{f_{cr,w}}} \tag{5}$$

$$f_{cr,w} = \frac{\pi^2 E}{\lambda_w^2} \tag{6}$$

$$\lambda_w = \frac{l_{eff}\sqrt{12}}{t_w} \tag{7}$$

In which l_{eff} is the effective length of web-post, b_w is the width of the web post, D_o is the opening diameter, χ is the reduction factor, $\bar{\lambda}$ is the reduced slenderness factor, λ_w is the web slenderness ratio and $f_{cr,w}$ is the critical stress at web post. Thus, the vertical shear strength can be calculated (**Eq. 8**):

$$V_{Lv,Rk} = \sigma_{Rk} t_w b_w \tag{8}$$

Panedpojaman et al. [13] made an adaptation in the effective length of the web post. In this model, the web post effective length is multiplied by a factor k (**Eqs. 9-10**):

$$l_{eff,P} = k\left(0.5\sqrt{p^2 - D_o^2}\right) \tag{9}$$

$$k = 0.9\left(\frac{p}{D_o}\right)\left(\frac{D_o}{d}\right)^2 \leq \min\left(1.15\frac{D_o}{d}, 1.15\right) \tag{10}$$

3. FINITE ELEMENT MODEL: VALIDATION STUDY

The numerical models are developed in two steps: elastic (buckling) and inelastic (post-buckling) [15,17,45–49]. The first step is used to estimate critical buckling loads on structures, and it can also be used as the first step to start the inelastic analysis. In the elastic analysis, no imperfections, physical and geometrical, are considered. The inelastic analysis is performed considering an initial geometric imperfection of d_g/1000. Using this imperfection factor (d_g/1000), in Ferreira et al. [17] sensitivity analyses were carried out using the finite element method, with the imperfection factor varying from d_g/100, d_g/200, d_g/250, d_g/500 and d_g/1000. The authors concluded that there was little sensitivity in the results, since the ultimate behavior was determined by the WPB. This low sensitivity in the results was assessed, also in Chen and Jia [50], and Couto and Vila Real [51]. The true initial imperfections of the cellular beams are a difficult task to determine, due to the manufacturing process [13]. In addition, in the case of cellular beams, the initial geometric imperfection in the web amount must not be greater than 4mm for sections with d_g<600mm and d_g/100 for sections with d_g>600 mm [52]. Therefore, for the present study, the factor of d_g/1000 is considered, according to the study presented in [17]. In this scenario, the deformed structure in the elastic analysis multiplied by an initial geometric imperfection scale factor is adopted as the shape at the beginning of this analysis. The implementation of geometric imperfection is performed using the command *INITIAL CONDITIONS of the ABAQUS® computational package [53]. **Table 2** shows the physical and geometric properties of the tests that are used in the validation study.

Table 2: Models (in mm, MPa and GPa)

Model	Ref	d_g	D_o	p	Upper tee					Lower tee				
					b_f	t_f	t_w	f_y (flange/web)	f_u (flange/web)	b_f	t_f	t_w	f_y (flange/web)	f_u (flange/web)
CCB1	[37]	575	375	500	141.8	8.6	6.4	312	438.5	141.8	8.6	6.4	312	438.5
CCB2	[37]	630	450	630	141.8	8.6	6.4	312	438.5	152.4	10.9	7.6	312	438.5
CCB3	[36]	555	380	570	180	13.5	8.6	451/489	541/587	180	13.5	8.6	451/489	541/587
CCB4	[36]	485	380	570	150	10.7	7.1	407/467	524/588	300	21.5	12	453/488	519/582

Model	Ref	E	Slab		L_b	L_p
			f_c	b		
CCB1	[37]	200	28.6	1200	4500	1750
CCB2	[37]	200	28.6	1200	4500	2250
CCB3	[36]	195	33.6	1800	6840*	1140/2850
CCB4	[36]	195	24.0	1800	6840*	1140/2850

*Slab cut back by 285 mm at end of cellular beam

3.1 MATERIALS

Regarding the constitutive material models, the quadrilinear model (**Fig. 2**) presented in Yun and Gardner [54] was used for steel **Eqs. (11-15)**. The implementation of the stress- strain relationship must be done with the real values, according to the **Eqs. (16-17).**

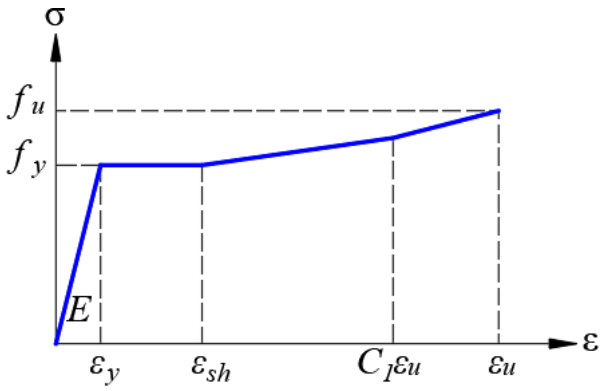

Fig. 2: Stress-strain relationship for steel [54]

$$f(\varepsilon)=\begin{cases} E\varepsilon, \varepsilon \le \varepsilon_y \\ f_y, \varepsilon_y < \varepsilon \le \varepsilon_{sh} \\ f_y + E_{sh}(\varepsilon-\varepsilon_{sh}), \varepsilon_{sh} < \varepsilon \le C_1\varepsilon_u \\ f_{C_1\varepsilon_u} + \left(\dfrac{f_u + f_{C_1\varepsilon_u}}{\varepsilon_u - C_1\varepsilon_u}\right), C_1\varepsilon_u < \varepsilon \le \varepsilon_u \end{cases} \quad (11)$$

$$\varepsilon_u = 0.6\left(1-\frac{f_y}{f_u}\right), \varepsilon_u \ge 0.06 \quad (12)$$

$$\varepsilon_{sh} = 0.1\frac{f_y}{f_u} - 0.055, 0.015 < \varepsilon_{sh} \le 0.03 \quad (13)$$

$$C_1 = \frac{\varepsilon_{sh} + 0.25\left(\varepsilon_u - \varepsilon_{sh}\right)}{\varepsilon_u} \tag{14}$$

$$E_{sh} = \frac{f_u - f_y}{0.4\left(\varepsilon_u - \varepsilon_{sh}\right)} \tag{15}$$

$$\sigma^{true} = \sigma^{nom}\left(1 + \varepsilon^{nom}\right) \tag{16}$$

$$\varepsilon^{true} = \ln\left(1 + \varepsilon^{nom}\right) \tag{17}$$

For concrete, the Carreira and Chu [55,56] model was adopted (**Eqs. 18-20**). The parameters that control plasticity yield criteria were similar to those presented in [17,48], according to **Table 3**.

$$\frac{\sigma}{f_c} = \frac{\beta_c\left(\varepsilon / \varepsilon_c\right)}{\beta_c - 1 + \left(\varepsilon / \varepsilon_c\right)^{\beta_c}} \tag{18}$$

$$\frac{\sigma}{f_t} = \frac{\beta_c\left(\varepsilon / \varepsilon_t\right)}{\beta_c - 1 + \left(\varepsilon / \varepsilon_t\right)^{\beta_c}} \tag{19}$$

$$\beta_c = \left(\frac{f_c}{32.4}\right)^3 + 1.55 \ \ (MPa) \tag{20}$$

Table 3: CDP input parameters

Parameter	Value
Ψ (º)	40
ξ	0.1 (default)
σ_{b0}/σ_{c0}	1.16 (default)
K_c	2/3 (default)
μ (s^{-1})	0.001

3.2 INTERACTION

About the interaction between the contact surfaces, the same strategy applied in [17,48,49,57,58] was used (**Fig. 3**). According to illustration, tie constraint, which is a restriction that represent the perfect bond between the surfaces, was applied to the surface between the shear connectors and the upper flange. Normal and tangential behavior (surface-to-surface) between the slab-connector and slab-beam are considered. The value of the friction coefficients was to 0.2 and 0.3 for slab-connector and slab-beam, respectively [59].

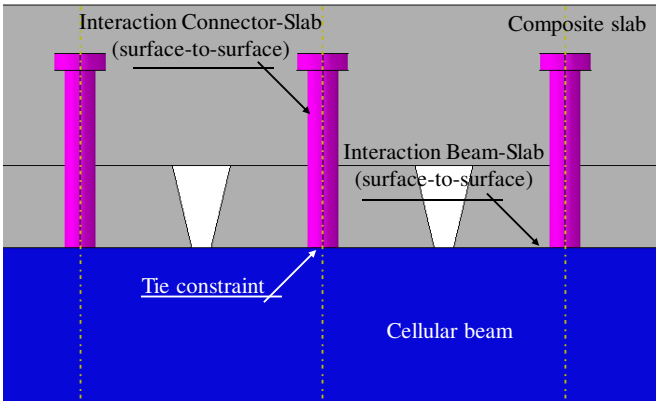

Fig. 3: Interaction of contact surfaces [17]

3.3 BOUNDARY CONDTIONS AND DISCRETIZATION

The boundary conditions were applied considering the symmetry at the longitudinal axis. **Fig. 4** illustrate the boundary conditions and discretization. The vertical displacement (U_y=0) in the support, and lateral displacement (Ux=0) at the ends of the slab were restrained. Longitudinal symmetry was applied at mid-span (U_z=U_{Rx}=U_{Ry}=0). About the discretization, the dimension of the elements was taken according to previous studies [60–62] respecting the master and slave surfaces. The cellular beam was discretized with shell-type finite elements (S4R). The headed stud connectors and the concrete slab were discretized by the solid element (C3D8R). Both elements have six degrees of freedom per node - three rotations and three translations. The validation results are presented by global shear curves by mid-span vertical displacement. Both the results of the elastic and inelastic analysis are illustrated.

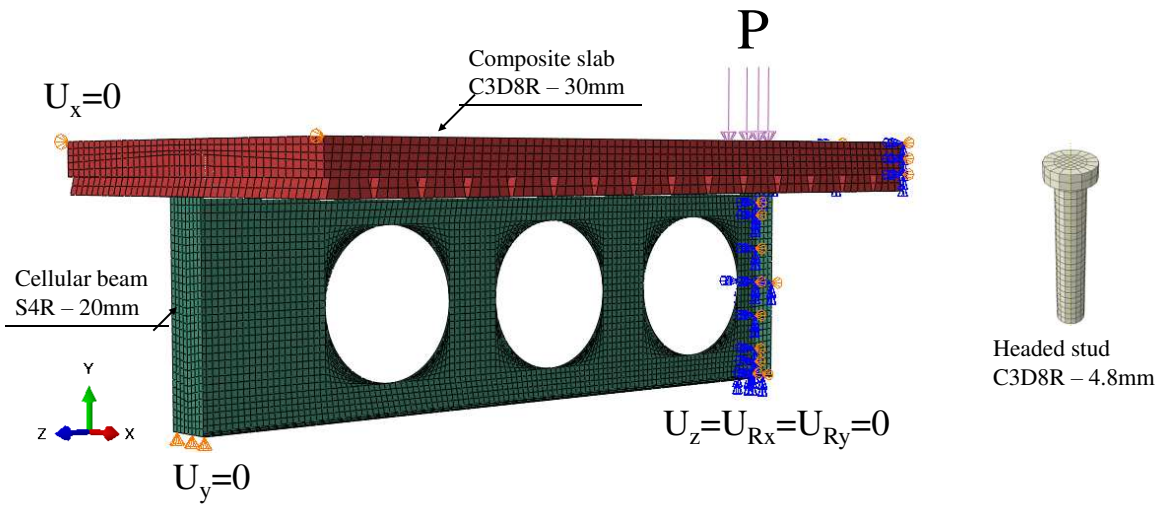

Fig. 4: Boundary conditions and discretization

3.4 VALIDATION RESULTS

The results of the validation study are presented below, considering the elastic and inelastic results (**Table 4** and **Fig. 5**). It is noteworthy that the elastic analysis is the first step to carry out the inelastic analysis, as previously described. It is observed in **Table 4** that the difference between the two analyses can reach up to 50%, since in the elastic analysis no initial imperfections are considered. In **Fig. 5** the curves of both analyses are shown compared to the tests. The response of the elastic analysis is presented by means of a constant line of blue color, since the ABAQUS software provides, for this type of analysis, eigenvalues and eigenvectors. According to the presentation of the results, it is possible to state that the numerical model is validated.

Table 4: Summary of results

Model	V_{Test} (kN)	$V_{FE,ELASTIC}$ (kN)	$V_{FE,INELASTIC}$ (kN)	$V_{FE,ELASTIC}/V_{FE,INELASTIC}$	$V_{FE}/V_{INELASTIC}$
CCB1	185	240	187	1.28	1.01
CCB2	215	263	213	1.23	0.99
CCB3	403	551	404	1.36	1.00
CCB4	329	492	328	1.50	1.00

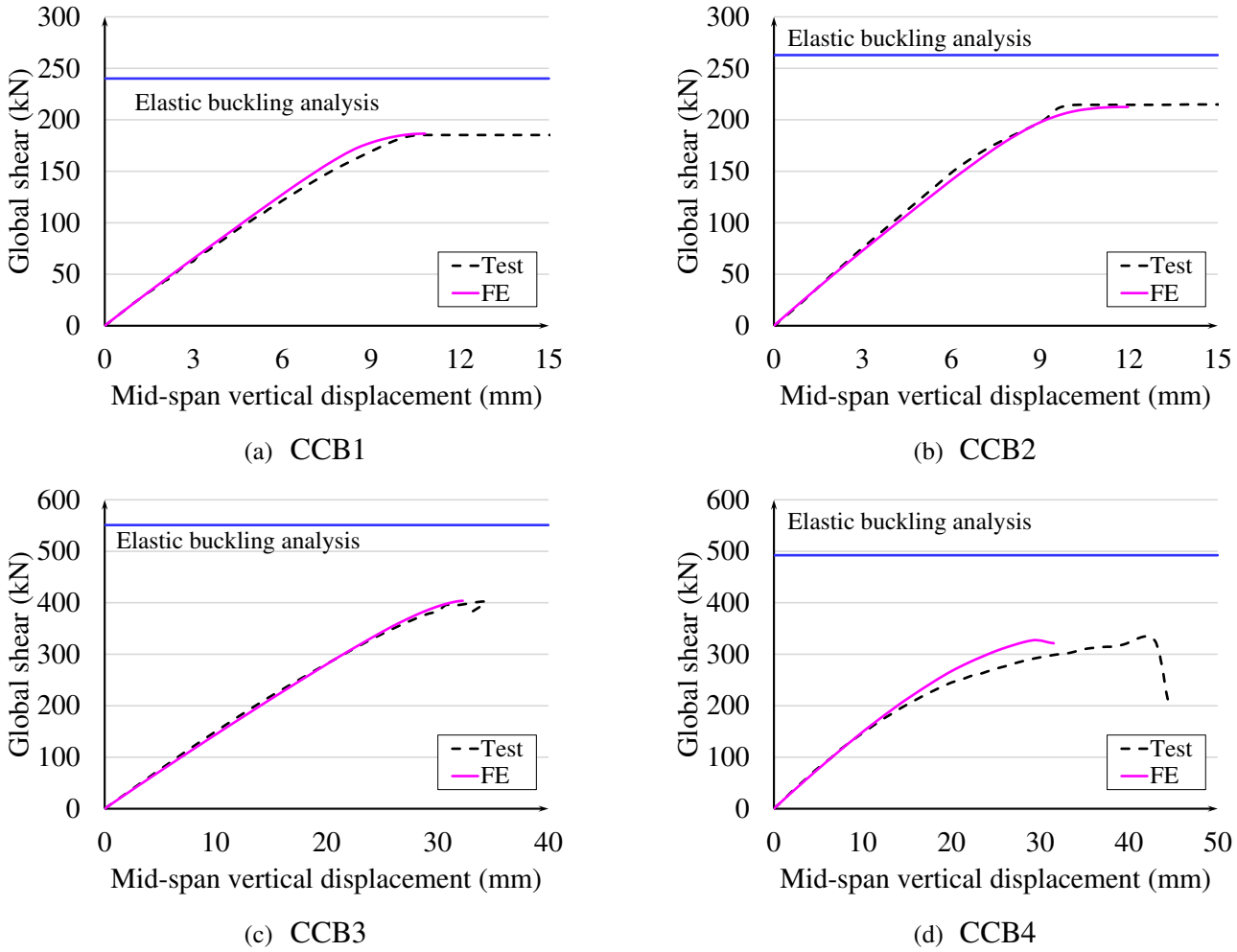

Fig. 5: Validation results

4. FINITE ELEMENT MODEL: PARAMETRIC STUDY

The following are the general considerations:

1. Six sections are considered (**Table 5**);

Table 5: Sections analyzed

Model	d_g	Upper tee			Lower tee		
		b_f	t_f	t_w	b_f	t_f	t_w
CCB1	575	141.8	8.6	6.4	141.8	8.6	6.4
CCB2	630	141.8	8.6	6.4	152.4	10.9	7.6
CCB3	555	180	13.5	8.6	180	13.5	8.6
CCB4	485	150	10.7	7.1	300	21.5	12
CCB5	580	180	13.5	8.6	180	13.5	8.6
CCB6	580	180	13.5	8.6	300	21.5	12

2. The ratios p/D_o and D_o/d are varied in 1.2-1.5 and 0.8-1.2, respectively;
3. The end post width (b_{we}) shall not be smaller than the other web posts width (b_w);
4. The length of the composite cellular beam is equal 6m, and the effective slab width is L/4;
5. The slab depth is equal to 150mm, with Holorib HR 51/150 geometry;
6. The headed stud dimension is 19x120mm;

7. The ASTM A572 Grade 50 steel is adopted (f_y=345 MPa and f_u=450 MPa). The Young's modulus is equal to 200 GPa;
8. The concrete resistance is 35 MPa for CCB1-4 sections, and 30 MPa for CCB5-6 sections;
9. The composite cellular beams are simply supported and subjected to two points of loads, spaced symmetrically in 2m from supports. Stiffeners were provided at the point of load and support.

5. RESULTS AND DISCUSSION

In total 120 analyses were performed. The results are discussed considering symmetric and asymmetric sections. At the end of each section, the results of elastic analysis are compared with the results of inelastic analysis [17]. At the end of the results and discussion section, a comparison between the numerical results with the critical global shear of the procedures is performed.

5.1. SYMMETRIC SECTION

This section discusses the results presented by sections CCB1, CCB3 and CCB4. In general, the buckling modes presented by section CCB1 were characterized by WPB. **Fig. 6** illustrates some examples. An important observation to be noted in **Fig. 6a** was the local web buckling at the end post. This phenomenon was observed for situations in which the end post width was much longer than the web post width.

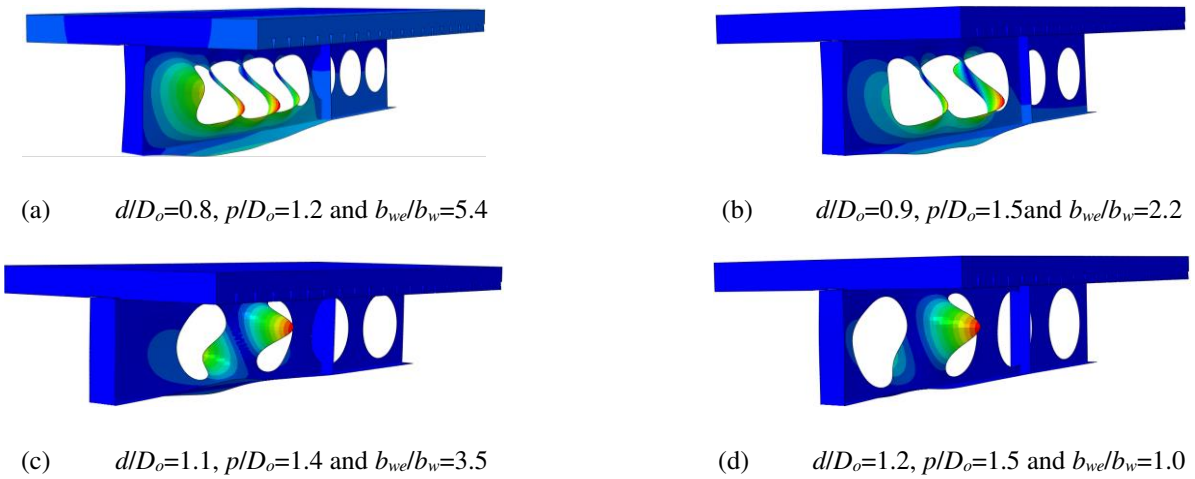

(a) d/D_o=0.8, p/D_o=1.2 and b_{we}/b_w=5.4 (b) d/D_o=0.9, p/D_o=1.5and b_{we}/b_w=2.2

(c) d/D_o=1.1, p/D_o=1.4 and b_{we}/b_w=3.5 (d) d/D_o=1.2, p/D_o=1.5 and b_{we}/b_w=1.0

Fig. 6: Buckling modes for CCB1 models

In **Fig. 7** the critical global shear curves (V_{cr}) are shown as a function of the key parameters (d/D_o and p/D_o). As noted, the curves for d/D_o=0.8, 0.9 and 1.1 showed a pattern. This is explained by the end post width, which presented similar values. In addition, the graph shows for these situations that the smaller the opening diameter, the greater the critical global shear that causes WPB. Also, as the web post width increases, the critical global shear tends to increase. On the other hand, for situations d/D_o=1.0 and 1.2, these values are divergent. In this scenario, the end post width was an important parameter that showed variability in the critical global shear. Such observations were measured for the b_{we}/b_w ratio approximately equal to 4.0.

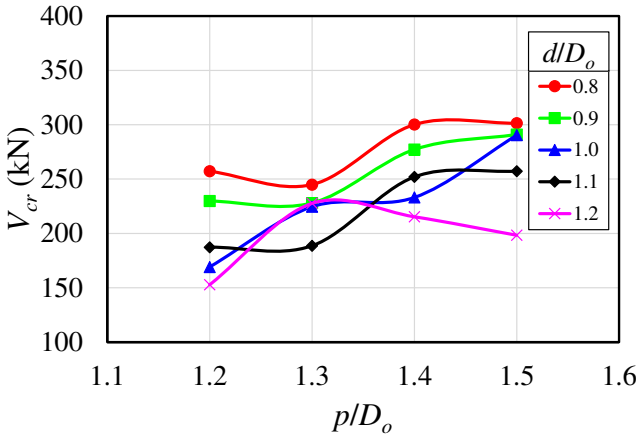

Fig. 7: Critical global shear vs. key parameters for CCB1 models

The behavior of the CCB3 (**Fig 8a-b**) and CCB5 (**Fig 8c-d**) models were similar to the behavior of the CCB1 model. This difference between the height of sections CCB3 and CCB5is 25mm, which was enough to change the buckling mode. As shown in **Fig. 8a**, the CCB3 model presented a buckling mode in which the local web buckling at the end post has been characterized. On the other hand, the CCB5 model did not show such buckling (**Fig. 8c**). This is explained by the fact that the model CCB5 presents the web slenderness greater than the model CCB3; a factor that transfers the local web buckling to the WPB. The results of the global critical shear as a function of the key parameters for the models CCB3 (**Fig. 9a**) and CCB5 are presented below (**Fig. 9b**). In this scenario, it is observed that the curve behaviors are similar to the CCB1 model. This is due to the fact that the diameter and the web post width have the same values as in the parametric study. For better visualization, in **Fig. 10** the results of each variation are presented for sections CCB1, CCB3 and CCB5. A difference of approximately 300kN is observed among sections CCB1 and CCB3 and CCB1 and CCB5. This difference is due to the fact that the CCB1 section has a higher slenderness value than the other sections. In addition, sections CCB3 and CCB5 have a web thickness equal to 8.6mm, while section CCB1 has a web thickness value of 6.4mm. Both parameters discussed are fundamental for the resistance to WPB, as presented in [13,18,63]. In relation to sections CCB3 and CC5, it is noted that the total height of the cellular beam causes small differences in critical global shear from the parameters d/D_o=0.9, p/D_o=1.4 (**Fig. 10b**). From this situation to the other parameters, the CCB3 model presented higher critical global shear results than the CCB5 section, due to the web slenderness of the CCB3 section being smaller than the CCB5 section.

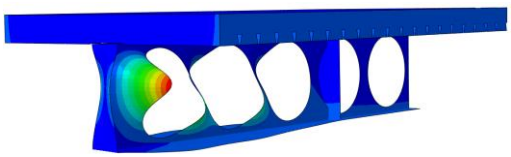

(a) CCB3: d/D_o=1.2, p/D_o=1.2 and b_{we}/b_w=1.8

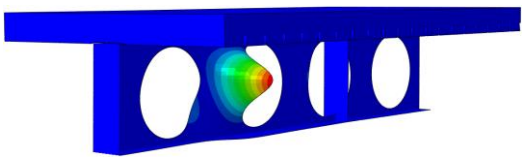

(b) CCB3: d/D_o=1.2, p/D_o=1.5 and b_{we}/b_w=1.0

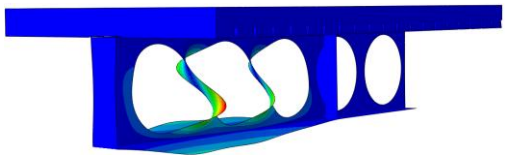

(c) CCB5: d/D_o=1.2, p/D_o=1.2 and b_{we}/b_w=1.8

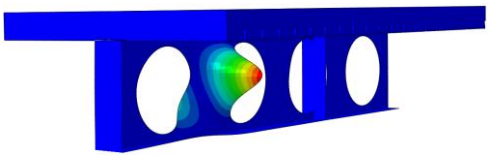

(d) CCB5: d/D_o=1.2, p/D_o=1.5 and b_{we}/b_w=1.0

Fig. 8: Buckling modes for models CCB3 and CCB5

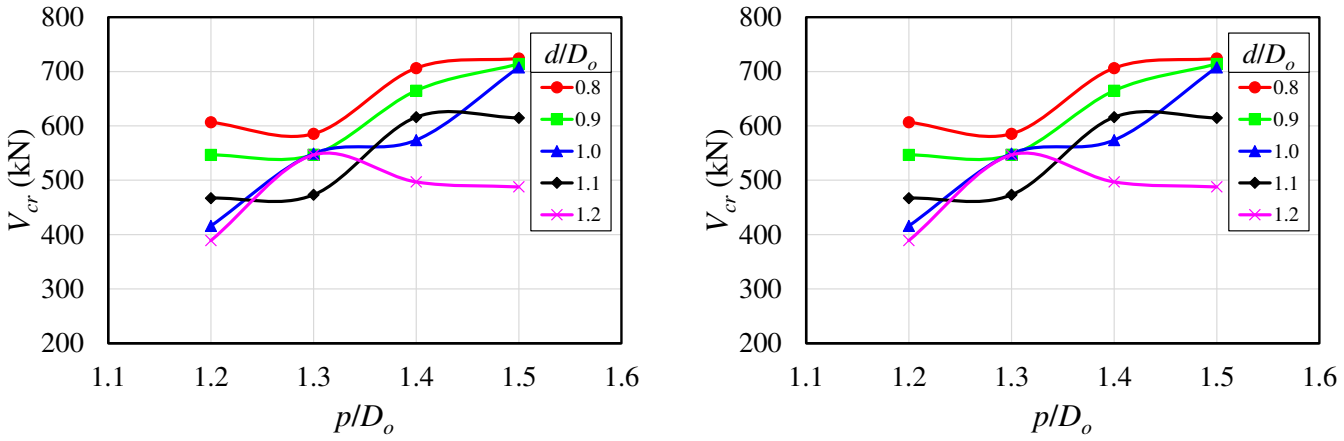

(a) CCB3 model (b) CCB5 model

Fig. 9: Critical global shear vs. key parameters for CCB3 and CCB5 models

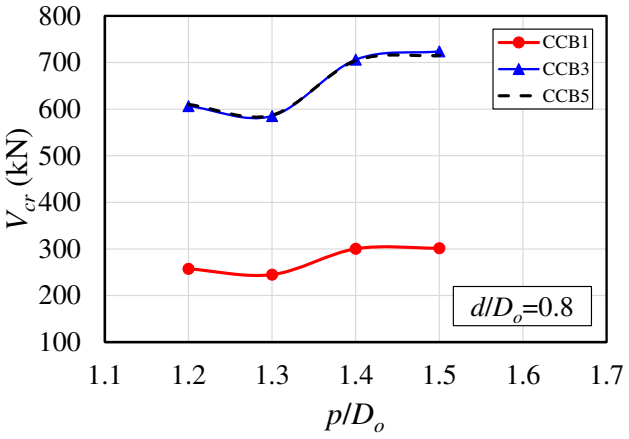

(a) d/D_o=0.8

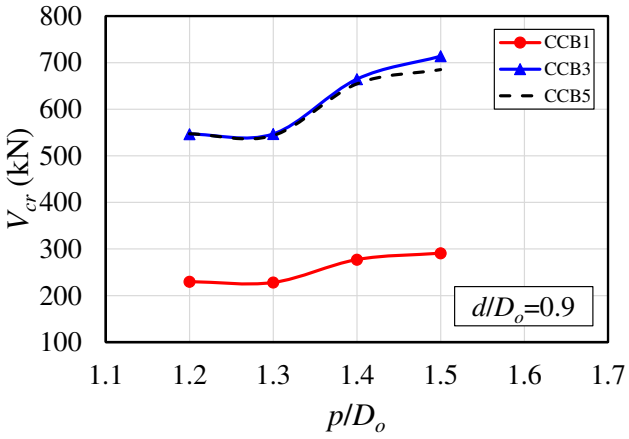

(b) d/D_o=0.9

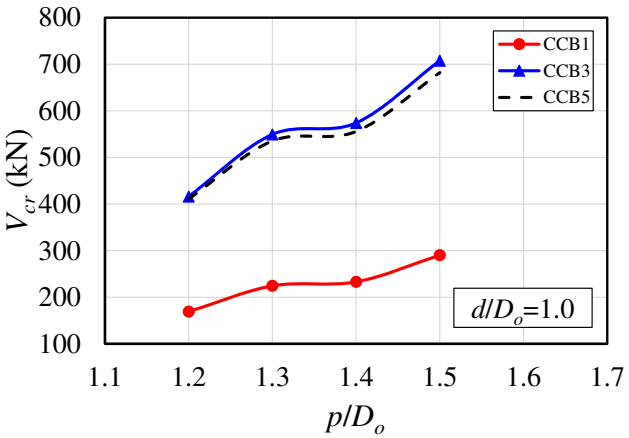

(c) d/D_o=1.0

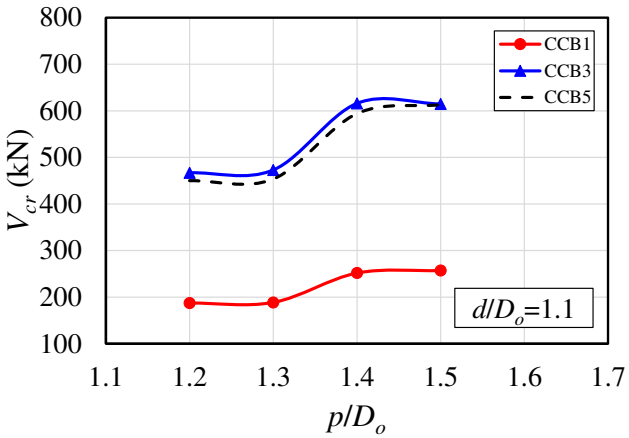

(d) d/D_o=1.1

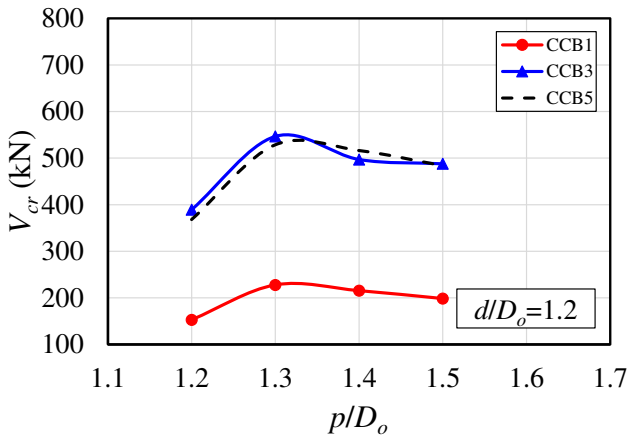

(e) d/D_o=1.2

Fig. 10: Comparative analyses for symmetric composite cellular beams

In **Fig. 11**, comparisons are presented between the elastic analyses of the present work, with the inelastic analyses presented by Ferreira et al. [17]. The differences, minimum, maximum and average were 11%, 51% and 36%, respectively. It is worth mentioning that in the elastic analysis, no physical and geometric imperfections are considered.

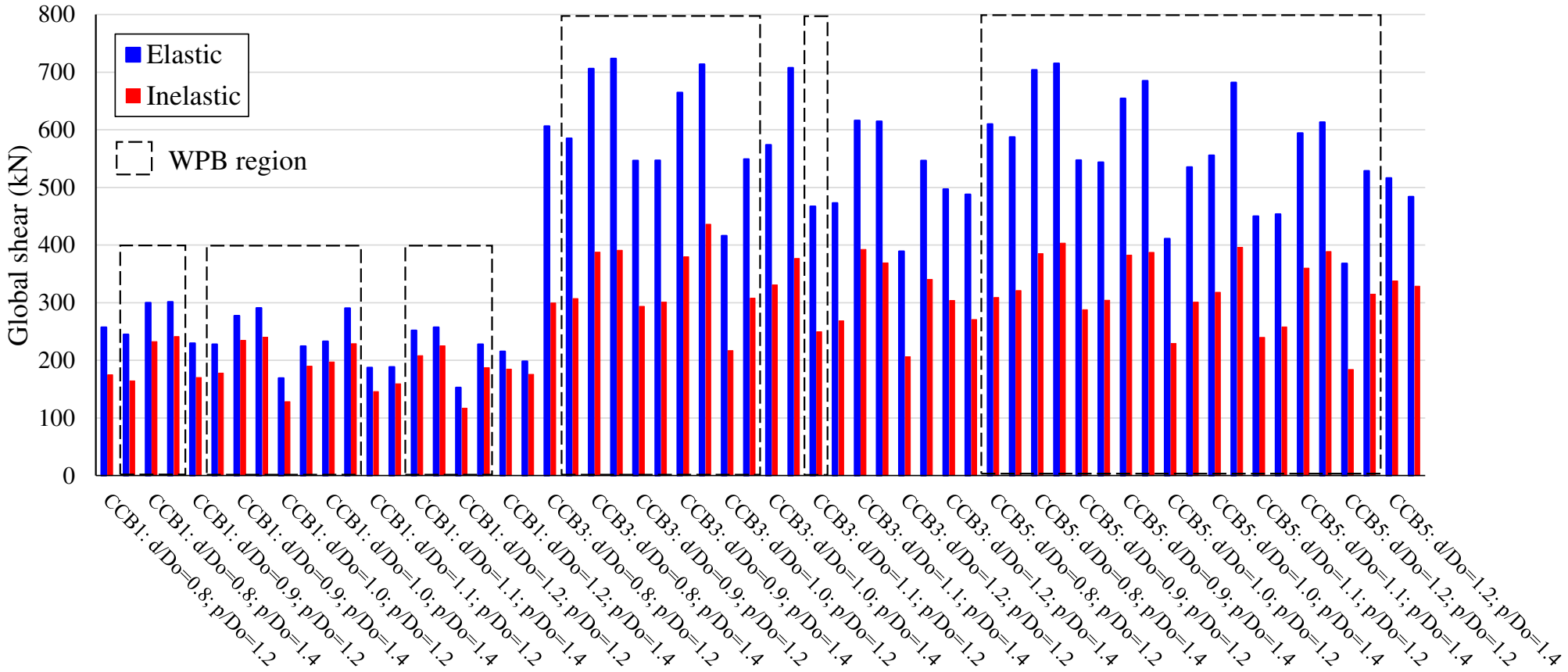

Fig. 11: Elastic and inelastic analyses for composite symmetric cellular beams

5.2. ASYMMETRIC SECTION

This section discusses the results presented by sections CCB2, CCB4 and CCB6. Regarding the CCB2 section, for some situations, the first buckling mode was not characterized by WPB (**Fig. 12**). As noted, the first buckling mode was characterized by local web buckling, specifically in the upper tee. This can be explained in relation to the lower tee being more rigid than the upper tee. Such buckling modes were observed for d/D_o=0.8. For other situations, WPB was verified. In **Fig. 13** some examples are presented. In **Fig. 14** the critical global shear curves (V_{cr}) are shown as a function of the key parameters (d/D_o and p/D_o). In the illustration, it is possible to observe a trend analogous to that previously presented for the symmetrical sections. This is possible due to the ratio between the areas of the upper tee to the lower tee being approximately 1.3, that is, a cross section with a low degree of asymmetry.

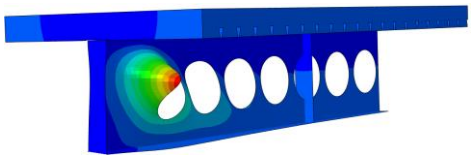

(a) d/D_o=0.8, p/D_o=1.2, b_{we}/b_w=5.4 and mode 1

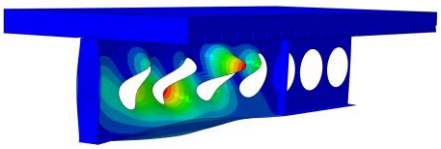

(b) d/D_o=0.8, p/D_o=1.2, b_{we}/b_w=5.4 and mode 2

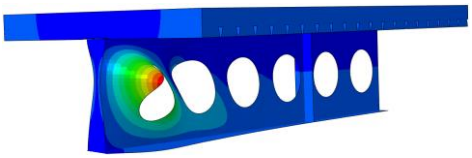

(c) d/D_o=0.8, p/D_o=1.5, b_{we}/b_w=1.3 and mode 1

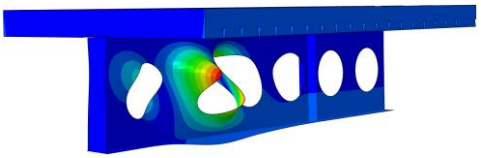

(d) d/D_o=0.8, p/D_o=1.5, b_{we}/b_w=1.3 and mode 2

Fig. 12: Buckling modes for CCB2 model

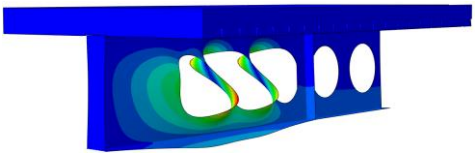

(a) d/D_o=0.9, p/D_o=1.4 and b_{we}/b_w=3.8

(b) d/D_o=1.0, p/D_o=1.2 and b_{we}/b_w=3.8

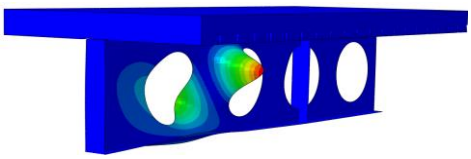

(c) d/D_o=1.1, p/D_o=1.5 and b_{we}/b_w=2.1

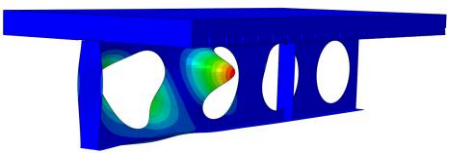

(d) d/D_o=1.5, p/D_o=1.5 and b_{we}/b_w=1.0

Fig. 13: WPB for CCB2 models

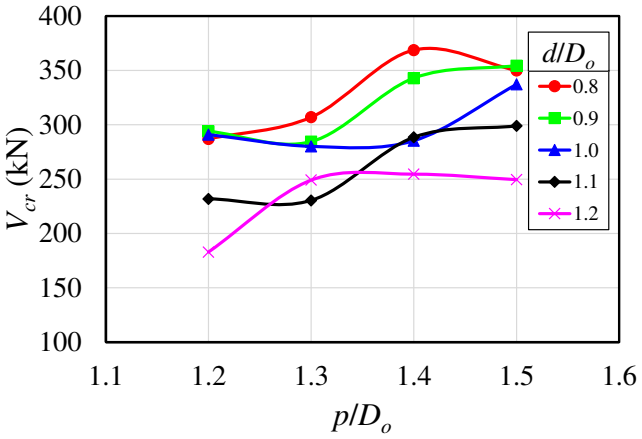

Fig. 14: Critical global shear vs. key parameters for CCB2 models

The buckling modes for sections CCB4 and CCB6, considering WPB, are illustrated below (**Fig. 15**). The sections CCB4 and CCB6 have the upper and lower tees formed by the sections IPE 300 and HEB 340, respectively. As shown in **Fig. 15a**, **Fig. 15c** and **Fig. 15d**, the WPB for the CCB4 section was characterized by the formation of a C-shaped buckling curvature in the upper tee, due to the lower tee being more rigid. Notably, for section CCB6 (**Fig. 15b**, **Fig. 15d** and **Fig. 15f**), the WPB was characterized by a double "S" shaped buckling curvature. What differs the section CCB4 and CCB6 is a variation of the total height of the cellular profile in approximately 100mm, that is, the section CCB6 is slenderer than the section CCB4.

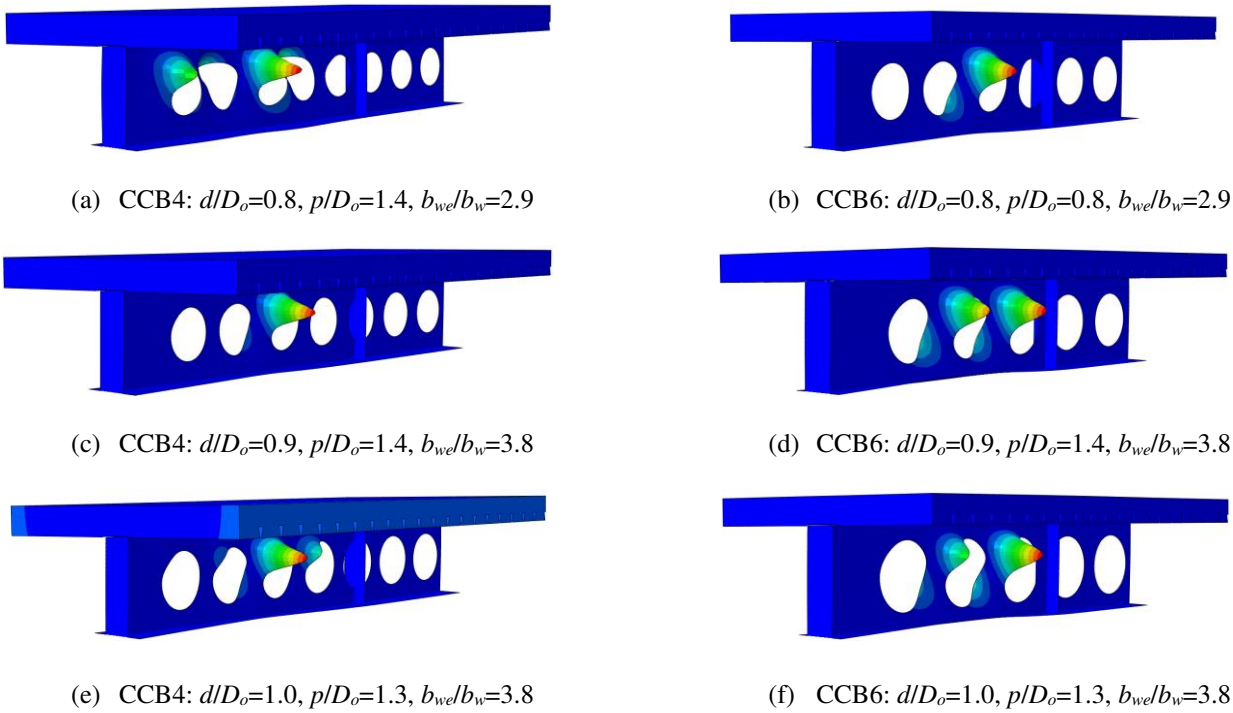

(a) CCB4: d/D_o=0.8, p/D_o=1.4, b_{we}/b_w=2.9

(b) CCB6: d/D_o=0.8, p/D_o=0.8, b_{we}/b_w=2.9

(c) CCB4: d/D_o=0.9, p/D_o=1.4, b_{we}/b_w=3.8

(d) CCB6: d/D_o=0.9, p/D_o=1.4, b_{we}/b_w=3.8

(e) CCB4: d/D_o=1.0, p/D_o=1.3, b_{we}/b_w=3.8

(f) CCB6: d/D_o=1.0, p/D_o=1.3, b_{we}/b_w=3.8

Fig. 15: WPB for CCB4 and CCB6 sections

Another important observation to be highlighted is in relation to the buckling modes. Alike section CCB2, for sections CCB4 and CCB6, it was verified that WPB did not occur in the first buckling mode. This occurred for several situations in section CCB4 (d/D_o=0.8, p/D_o=1.2-1.3 and 1.5; d/D_o=0.9, p/D_o=1.2-1.3 and 1.5; d/D_o=1.0, p/D_o=1.2 and 1.4-1.5; d/D_o=1.1-1.2, p/D_o=1.2-1.5), which is less slender than the CCB6 section. For the CCB6 section, these situations were observed only for d/D_o=0.8 and

p/D_o=1.2-1.3 and 1.5 models. **Fig. 16 and Fig. 17** illustrates some examples. When this occurs, the ultimate behavior of inelastic analysis is governed by a plastic mechanism or even the rupture of the shear connectors [17]. The results of the global critical shear as a function of the key parameters for the models CCB4 (**Fig. 18a**) and CCB6 are presented below (**Fig. 18b**).

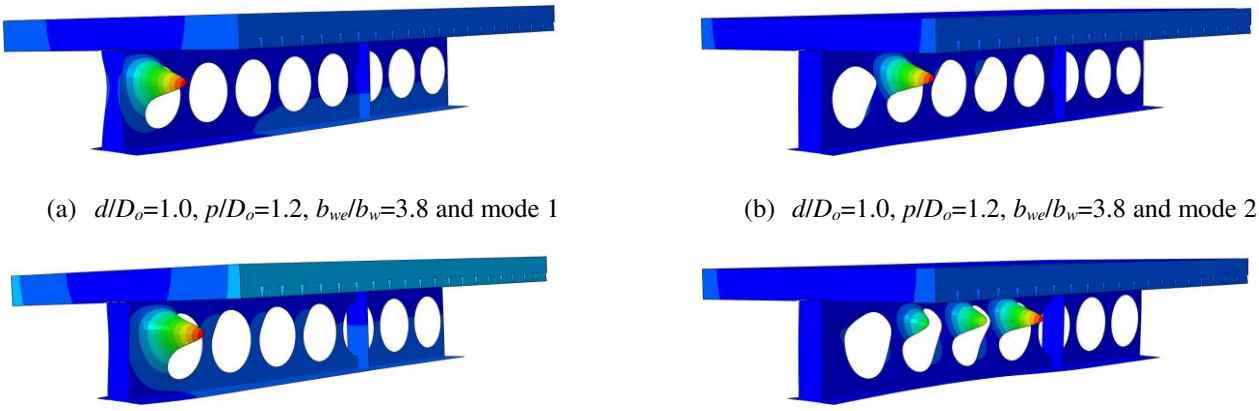

(a) d/D_o=1.0, p/D_o=1.2, b_{we}/b_w=3.8 and mode 1

(b) d/D_o=1.0, p/D_o=1.2, b_{we}/b_w=3.8 and mode 2

(c) d/D_o=1.1, p/D_o=1.2, b_{we}/b_w=4.6 and mode 1

(d) d/D_o=0.8, p/D_o=1.5, b_{we}/b_w=4.6 and mode 2

Fig. 16: Buckling modes for CCB4 model

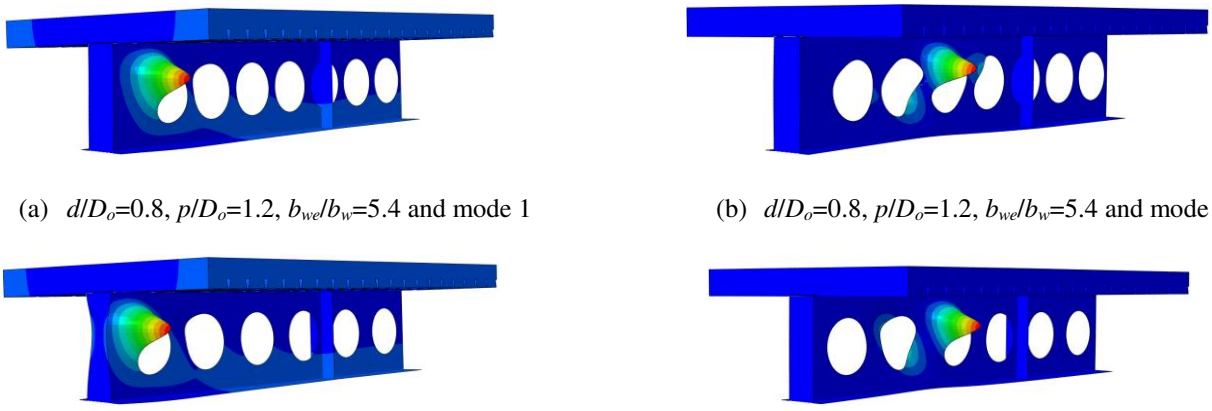

(a) d/D_o=0.8, p/D_o=1.2, b_{we}/b_w=5.4 and mode 1

(b) d/D_o=0.8, p/D_o=1.2, b_{we}/b_w=5.4 and mode 2

(c) d/D_o=0.8, p/D_o=1.5, b_{we}/b_w=1.3 and mode 1

(d) d/D_o=0.8, p/D_o=1.5, b_{we}/b_w=1.3 and mode 2

Fig. 17: Buckling modes for CCB6 model

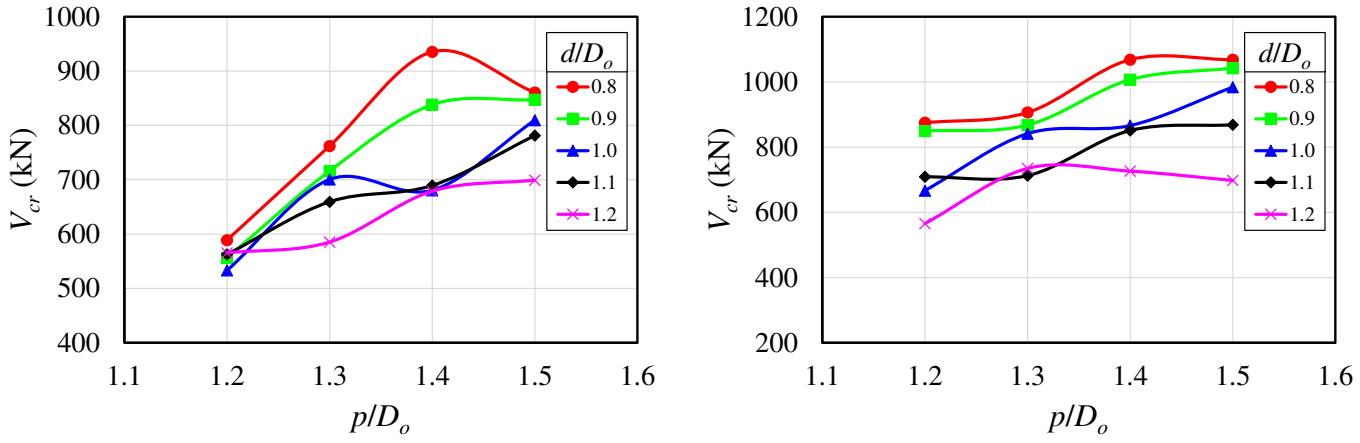

(a) CCB4 model

(b) CCB6 model

Fig. 18: Critical global shear vs. key parameters for CCB4 and CCB6 models

As noted, the CCB4 section, which is less slender than the CCB6 section, showed lower values of critical global shear (**Fig. 18a**). This is explained by the occurrence of local web buckling of the upper tee. Notably, for section CCB6 (**Fig. 18b**) the values of the critical global shear were higher, because in most situations the WPB was verified, thus requesting both the upper and lower tees. **Fig. 19** shows the comparisons between sections CCB2, CCB4 and CCB6, and **Fig. 20**, comparisons are presented between the elastic analyses of the present work, with the inelastic analyses presented by Ferreira et al. [17].

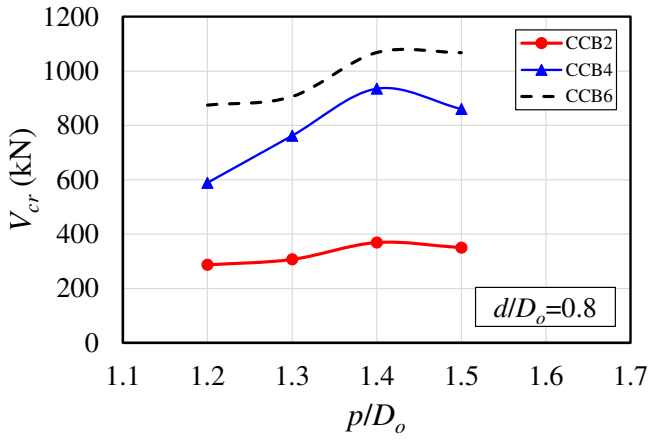

(a) d/D_o=0.8

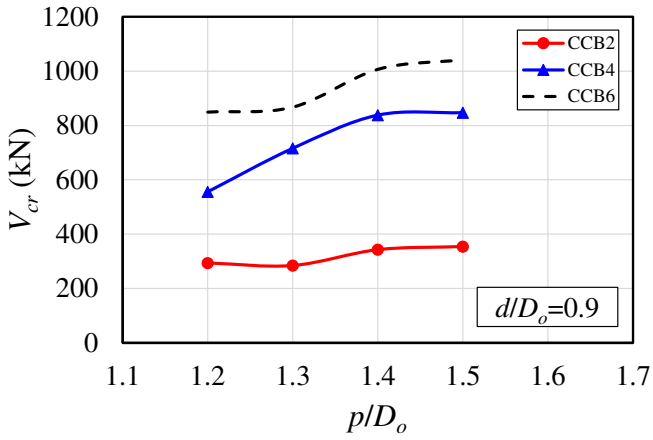

(b) d/D_o=0.9

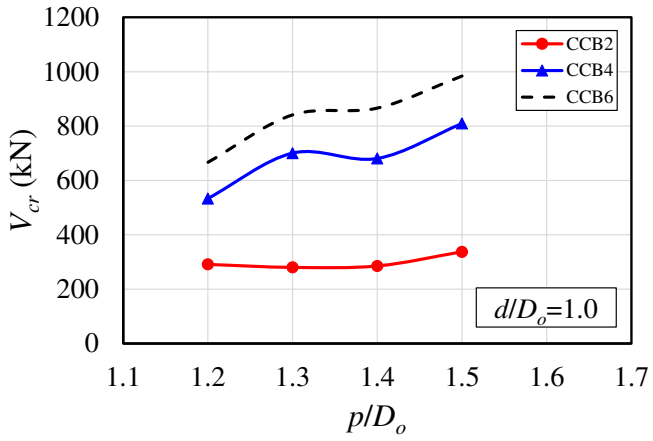

(c) d/D_o=1.0

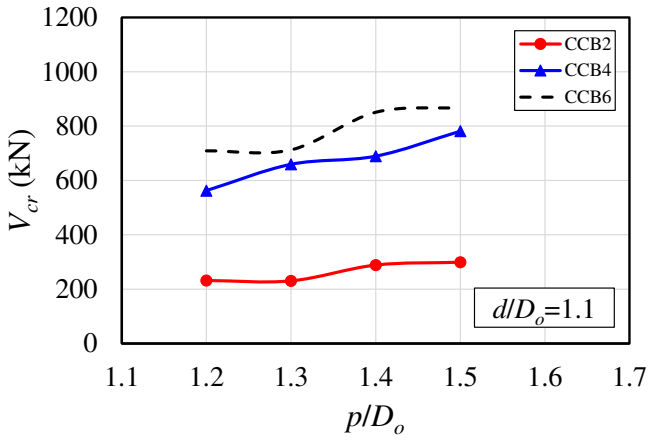

(d) d/D_o=1.1

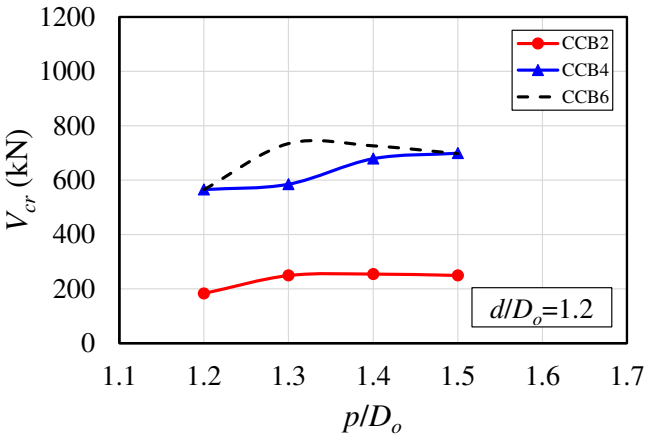

(e) d/D_o=1.2

Fig. 19: Comparative analyses for asymmetric composite cellular beams

The differences, minimum, maximum and average were 8%, 53% and 39%, respectively. It is worth mentioning that in the elastic analysis, no physical and geometric imperfections are considered.

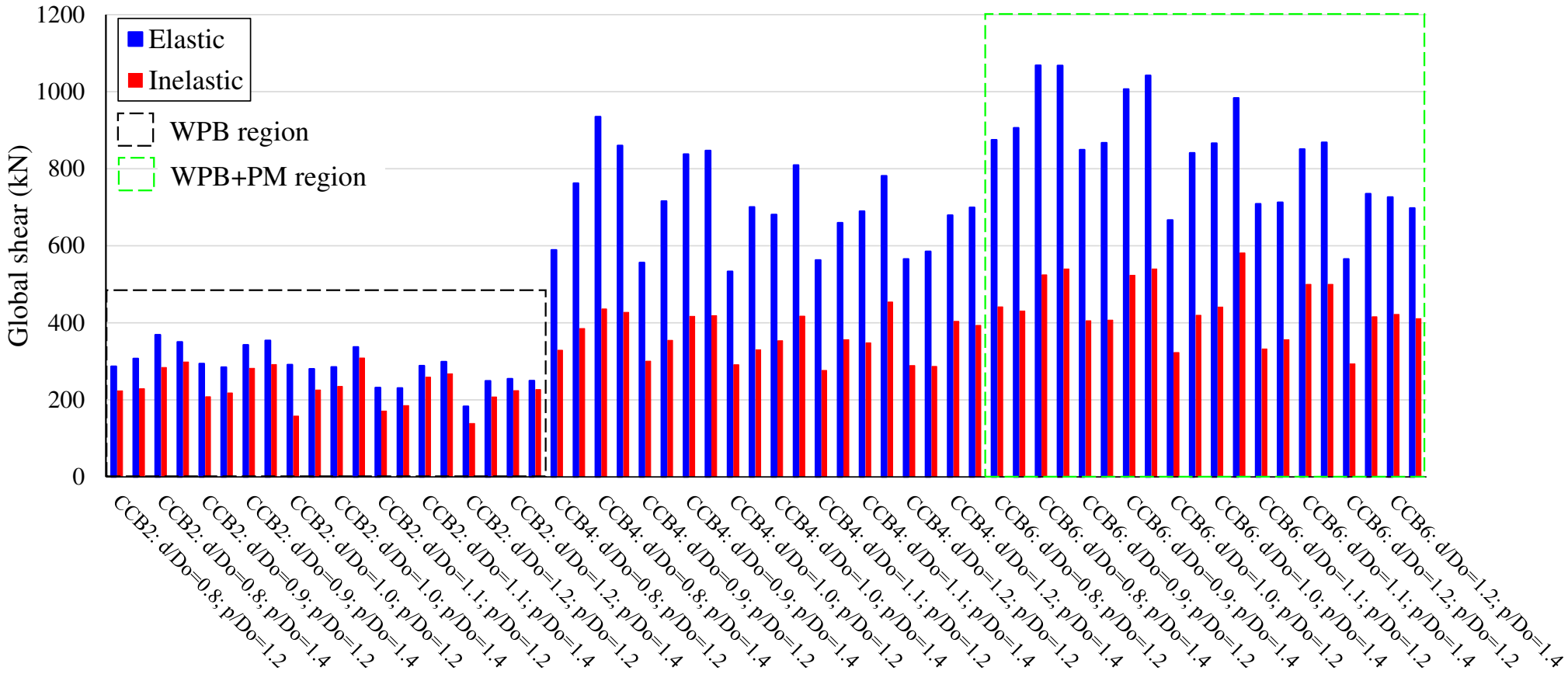

Fig. 20: Elastic and inelastic analyses for composite asymmetric cellular beams

5.3. STATISTICAL ANALYSIS

The results of the elastic analyses are presented according to each key parameter, such as the relationships d/D_o, p/D_o and b_{we}/b_w, considering all sections analyzed (**Fig. 21**). As shown in **Fig. 21a**, in general, the smaller the opening diameter, the greater the critical global shear that causes WPB. It is noteworthy that the smaller the opening diameter, the larger the tees sections. According to **Fig. 21b**, the greater the web post width, the greater the critical global shear response. Finally, on the variation of the end post (**Fig. 21c**), the greatest influence was measured for the sections that presented greater web thickness (CCB3-CCB6) and asymmetry (CCB4 and CCB6).

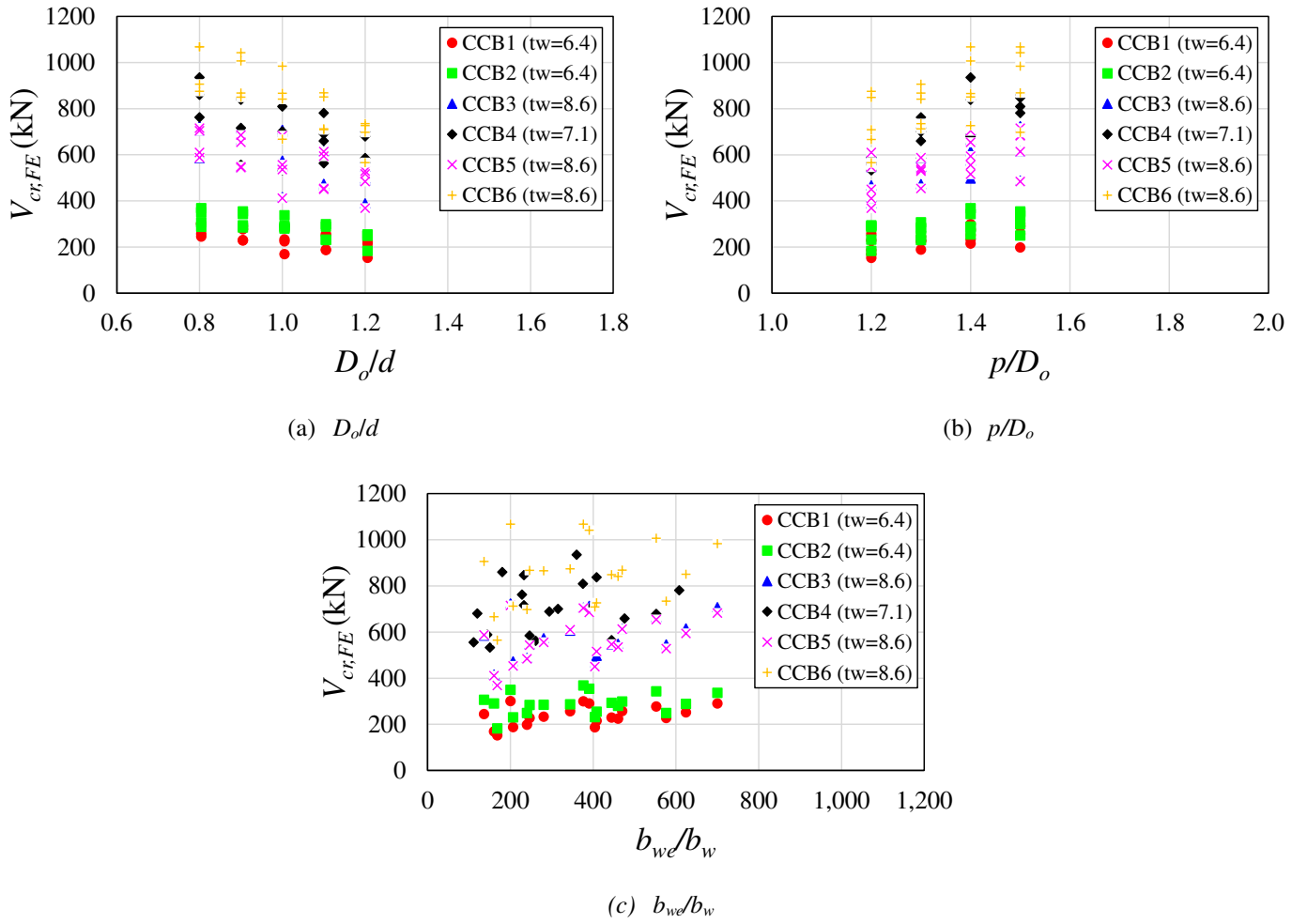

(a) D_o/d (b) p/D_o

(c) b_{we}/b_w

Fig. 21: The influence of key parameters on critical global shear

Fig. 22 depicts a comparison of the critical global shear with the analytical procedures presented in section 2. As shown, a greater conformity between the elastic numerical values was verified with the procedure of Panedpojaman et al. [13]. This meant that in total 101 observations were in the conservative zone ($V_{cr}/V_{cr,FE} \leq 1.0$). Thus, such a procedure, which takes into account the k factor for the calculation of the effective length, is a good approximation for the estimation of the elastic buckling. On the other hand, the procedure prescribed in SCI P355 [18] overestimated the elastic analysis, since all results showed $V_{cr}/V_{cr,FE} > 1.0$. This conclusion, also, was stated in Abrambes et al. [14] and Rajana et al. [15], considering non-composite cellular beams.

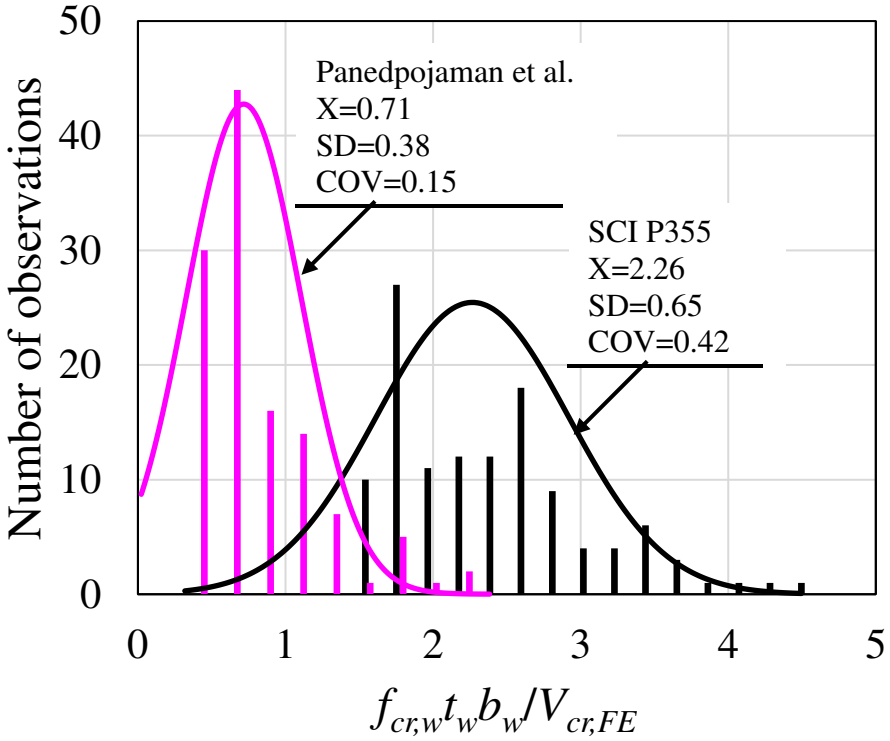

Fig. 22: Statistical analysis

Another observation to be considered is illustrated in **Fig. 23**. Such an illustration normalizes the results of the elastic and inelastic analyses [17] for comparison with the EC3 buckling curves. As previously presented, the use of buckling curves *b* and *c* may underestimate the strength of composite cellular beams, since most of the results presented were above the buckling curve *a*.

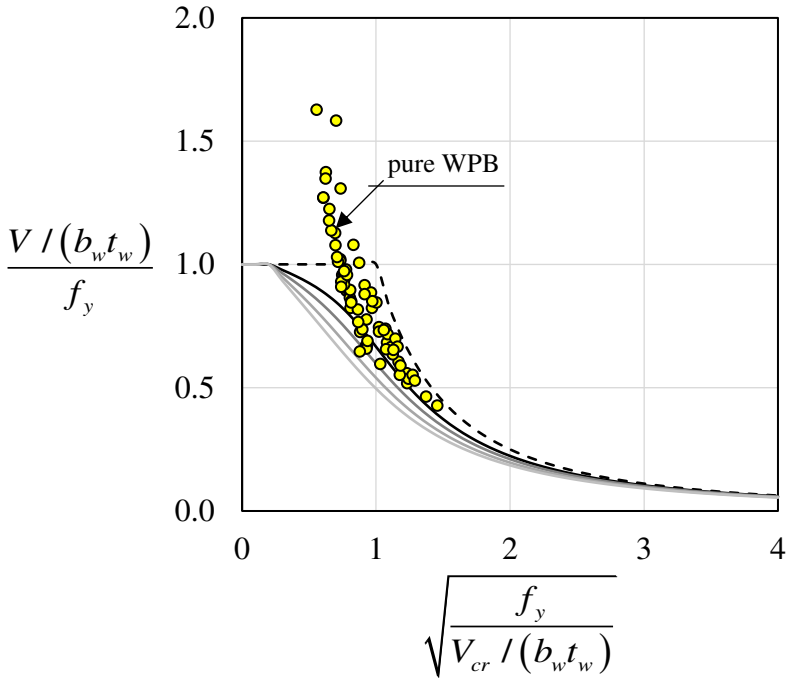

Fig. 23: Elastic and Inelastic analyses vs. EC3 buckling curves

CONCLUDING REMARKS

This paper presented a numerical model capable of representing experimental models of composite cellular beams. A parametric study was carried out, varying the cross sections as well as the d/D_o, p/D_o and b_{we}/b_w ratios. In total, 120 models were processed. The elastic analyses were compared with inelastic analyses and analytical procedures, considering the critical global shear that causes the web post buckling. It was concluded:

1. In composite cellular beams with a less slender web, local web buckling is observed in the upper tee close to the support;
2. Increasing the web slenderness, the buckling mode changed from local web buckling to web post buckling. This effect generated an increase in the critical global shear, as both upper and lower tees were utilized;
3. The smaller the opening diameter is, the greater the critical global shear that causes WPB;
4. The greater the web post width is, the greater the critical global shear;
5. The end post width is an expressive parameter that influences the critical global shear in composite asymmetric cellular beams with slender web;
6. The differences between elastic and inelastic analyses show an average value of 36% and 39%, for the composite symmetric and asymmetric sections, respectively.
7. The calculation procedure recommended by SCI P355 overestimates the elastic analyses, while the procedure that presents the modification of the effective length is a good approximation for the estimation of the elastic buckling.

ACKNOWLEDGMENTS

This work was supported by the São Paulo Research Foundation (FAPESP) [grant number #2018/22803-1].

REFERENCES

[1] El-Sawy KM, Sweedan AMI, Martini MI. Moment gradient factor of cellular steel beams under inelastic flexure. J Constr Steel Res 2014;98:20–34. https://doi.org/10.1016/j.jcsr.2014.02.007.

[2] Ellobody E. Nonlinear analysis of cellular steel beams under combined buckling modes. Thin-Walled Struct 2012;52:66–79. https://doi.org/10.1016/j.tws.2011.12.009.

[3] Panedpojaman P, Sae-Long W, Chub-Uppakarn T. Cellular beam design for resistance to inelastic lateral-torsional buckling. Thin-Walled Struct 2016;99:182–94. https://doi.org/10.1016/j.tws.2015.08.026.

[4] Redwood RG, Wong PK. Web holes in composite beams with steel deck. Can. Struct. Eng. Conf. -1982, Ontario, Toronto: Canadian Steel Construction Council; 1982, p. 1–41.

[5] Redwood RG, Poumbouras G. Tests of composite beams with web holes. Can J Civ Eng 1983;10:713–21. https://doi.org/10.1139/l83-100.

[6] Donahey RC, Darwin D. Web openings in composite beams with ribbed slabs. J Struct Eng 1988;114:518–34. https://doi.org/10.1061/(ASCE)0733-9445(1988)114:3(518).

[7] Park JW, Kim CH, Yang SC. Ultimate Strength of Ribbed Slab Composite Beams with Web Openings. J Struct Eng 2003;129:810–7. https://doi.org/10.1061/(asce)0733-9445(2003)129:6(810).

[8] Sheehan T, Dai X, Lam D, Aggelopoulos E, Lawson M, Obiala R. Experimental study on long spanning composite cellular beam under flexure and shear. J Constr Steel Res 2016;116:40–54. https://doi.org/10.1016/j.jcsr.2015.08.047.

[9] Erdal F, Saka MP. Ultimate load carrying capacity of optimally designed steel cellular beams. J Constr Steel Res 2013;80:355–68. https://doi.org/10.1016/j.jcsr.2012.10.007.

[10] Kerdal D, Nethercot DA. Failure modes for castellated beams. J Constr Steel Res 1984;4:295–315. https://doi.org/10.1016/0143-974X(84)90004-X.

[11] Redwood R, Cho SH. Design of steel and composite beams with web openings. J Constr Steel Res 1993;25:23–41. https://doi.org/10.1016/0143-974X(93)90050-3.

[12] Tsavdaridis KD, D'Mello C. Vierendeel Bending Study of Perforated Steel Beams with Various Novel Web Opening Shapes through Nonlinear Finite-Element Analyses. J Struct Eng 2012;138:1214–30. https://doi.org/10.1061/(asce)st.1943-541x.0000562.

[13] Panedpojaman P, Thepchatri T, Limkatanyu S. Novel design equations for shear strength of local web-post buckling in cellular beams. Thin-Walled Struct 2014;76:92–104. https://doi.org/10.1016/j.tws.2013.11.007.

[14] Abambres M, Rajana K, Tsavdaridis K, Ribeiro T. Neural Network-Based Formula for the Buckling Load Prediction of I-Section Cellular Steel Beams. Computers 2018;8:2. https://doi.org/10.3390/computers8010002.

[15] Rajana K, Tsavdaridis KD, Koltsakis E. Elastic and inelastic buckling of steel cellular beams under strong-axis bending. Thin-Walled Struct 2020;156:106955. https://doi.org/10.1016/j.tws.2020.106955.

[16] EUROPEAN COMMITTEE FOR STANDARDIZATION. Eurocode 3: Design of steel structures—Part 1-1: General rules and rules for buildings 2005.

[17] Ferreira FPV, Martins CH, De Nardin S. Assessment of web post buckling resistance in steel-concrete composite cellular beams. Thin-Walled Struct 2020:106969. https://doi.org/10.1016/j.tws.2020.106969.

[18] Lawson RM, Hicks SJ. Design of beams with large web openings. The Steel Construction Institute; 2011.

[19] Granade CJ. An investigation of composite beams having large rectangular openings in their webs. 1968. Partial M.Sc. thesis. University of Alabama, 1968.

[20] Clawson WC, Darwin D. Tests of composite beams with web openings. ASCE J Struct Div 1982;108:145–62.

[21] Cho SH. An investigation on the strength of composite beams with web openings. 1982. M.Sc. thesis. Hanyang University, 1982.

[22] Narayanan R, Al-Amery RIM, Roberts TM. Shear strength of composite plate girders with rectangular web cut-outs. J Constr Steel Res 1989;12:151–66. https://doi.org/10.1016/0143-974X(89)90030-8.

[23] Roberts TM, Al-Amery RIM. Shear strength of composite plate girders with web cutouts. J Struct Eng 1991;117:1897–910. https://doi.org/10.1061/(ASCE)0733-9445(1991)117:7(1897).

[24] Todd DM, Cooper PB. Strength of composite beams with web openings. ASCE J Struct Div 1980;106:431–44.

[25] DONOGHUE CM. Strength of composite beams with web openings. ASCE J Struct Div 1982;108:2652–67.

[26] Clawson WC, Darwin D. Strength of composite beams at web openings. ASCE J Struct Div 1982;108:623–41.

[27] Lawson RM, Chung KF, Price AM. Tests on composite beams with large web openings to justify existing design methods. Struct Enginee 1992;70:1–7.

[28] Cho SH, Redwood RG. Slab behavior in composite beams at openings. II: tests and verification. J Struct Eng 1992;118:2304–22. https://doi.org/10.1061/(ASCE)0733-9445(1992)118:9(2304).

[29] Redwood RG, Poumbouras G. Analysis of composite beams with web openings. J Struct Eng 1984;110:1949–58. https://doi.org/10.1061/(ASCE)0733-9445(1984)110:9(1949).

[30] Darwin D, Donahey RC. LRFD for composite beams with unreinforced web openings. J Struct Eng 1988;114:535–52. https://doi.org/10.1061/(ASCE)0733-9445(1988)114:3(535).

[31] Cho SH, Redwood RG. Slab behavior in composite beams at openings. I: analysis. J Struct Eng 1992;118:2287–303. https://doi.org/10.1061/(ASCE)0733-9445(1992)118:9(2287).

[32] Fahmy EH. Analysis of composite beams with rectangular web openings. J Constr Steel Res 1996;37:47–62. https://doi.org/10.1016/0143-974X(95)00022-N.

[33] Benitez MA, Darwin D, Donahey RC. Deflections of composite beams with web openings. J Struct Eng 1998;124:1139–47. https://doi.org/10.1061/(ASCE)0733-9445(1998)124:10(1139).

[34] Chung K. F, Lawson R. M. Simplified design of composite beams with large web openings to Eurocode 4. J Constr Steel Res 2001;57:135–64. https://doi.org/10.1016/S0143-974X(00)00011-0.

[35] Hechler O, Müller C, Sedlacek G. Investigations on Beams with Multiple Regular Web Openings. Compos. Constr. Steel Concr. V, Reston, VA: American Society of Civil Engineers; 2006, p. 270–81. https://doi.org/10.1061/40826(186)26.

[36] MÜLLER C, HECHLER O, BUREAU A, BITAR D, JOYEUX D, CAJOT LG, et al. Large web openings for service integration in composite floors. Technical Steel Research. European Comission, Contract No 7210-PR/315. Final report 2006.

[37] Nadjai A. Performance of cellular composite floor beams at ambient temperature. 2005.

[38] Nadjai A, Vassart O, Ali F, Talamona D, Allam A, Hawes M. Performance of cellular composite floor beams at elevated temperatures. Fire Saf J 2007;42:489–97. https://doi.org/10.1016/j.firesaf.2007.05.001.

[39] Gizejowski MA, Khalil WAS. Stability and ductility of castellated composite beams subjected to hogging bending. In: Batista E, Vellasco P, Lima L de, editors. SDSS'Rio 2010 Stab. DUCTILITY STEEL Struct., Rio de Janeiro: 2010, p. 839–46.

[40] EUROPEAN COMMITTEE FOR STANDARDIZATION. EN 1994-1-1: Eurocode 4 – Design of composite steel and concrete structures – Part 1-1: General rules for buildings. 2004.

[41] Fares SS, Coulson J, Dinehart DW. AISC Steel Design Guide 31: Castellated and Cellular Beam Design. American Institute of Steel Construction; 2016.

[42] Grilo LF, Fakury RH, Castro e Silva ALR de, Veríssimo G de S. Design procedure for the web-post buckling of steel cellular beams. J Constr Steel Res 2018;148:525–41. https://doi.org/10.1016/j.jcsr.2018.06.020.

[43] Ferreira FPV, Martins CH, De Nardin S. Advances in composite beams with web openings and composite cellular beams. J Constr Steel Res 2020;172:106182. https://doi.org/10.1016/j.jcsr.2020.106182.

[44] EUROPEAN COMMITTEE FOR STANDARDIZATION. EUROCODE 3: Design of steel structures - Part 1-1: General rules and rules buildings 2005.

[45] Ferreira FPV, Martins CH. LRFD for Lateral-Torsional Buckling Resistance of Cellular Beams. Int J Civ Eng 2020;18:303–23. https://doi.org/10.1007/s40999-019-00474-7.

[46] Ferreira FPV, Rossi A, Martins CH. Lateral-torsional buckling of cellular beams according to the possible updating of EC3. J Constr Steel Res 2019;153:222–42. https://doi.org/10.1016/j.jcsr.2018.10.011.

[47] Rossi A, Ferreira FPV, Martins CH, Mesacasa Júnior EC. Assessment of lateral distortional buckling resistance in welded I-beams. J Constr Steel Res 2020;166:105924. https://doi.org/10.1016/j.jcsr.2019.105924.

[48] Ferreira FPV, Martins CH, De Nardin S. Sensitivity Analysis of Composite Cellular Beams to Constitutive Material Models and Concrete Fracture. Int J Struct Stab Dyn 2020:2150008. https://doi.org/10.1142/S0219455421500085.

[49] Ferreira FPV, Martins CH, De Nardin S. A parametric study of steel-concrete composite beams with hollow core slabs and concrete topping. Structures 2020;28:276–96. https://doi.org/10.1016/j.istruc.2020.08.045.

[50] Chen S, Jia Y. Numerical investigation of inelastic buckling of steel–concrete composite beams prestressed with external tendons. Thin-Walled Struct 2010;48:233–42. https://doi.org/10.1016/j.tws.2009.10.009.

[51] Couto C, Vila Real P. Numerical investigation on the influence of imperfections in the lateral-torsional buckling of beams with slender I-shaped welded sections. Thin-Walled Struct 2019;145:106429. https://doi.org/10.1016/j.tws.2019.106429.

[52] ArcelorMittal. ACB® and Angelina® beams - A New Generation of Cellular Beams 2018.

[53] Dassault Systèmes Simulia. Abaqus 6.18 2016.

[54] Yun X, Gardner L. Stress-strain curves for hot-rolled steels. J Constr Steel Res 2017;133:36–46. https://doi.org/10.1016/j.jcsr.2017.01.024.

[55] Carreira DJ, Chu KH. Stress-Strain Relatonship for Reinforced Concrete in Tension. J Am Concr Inst 1986;83:21–8.

[56] CARREIRA DJ, CHU KH. Stress-Strain Relationship for Plain Concrete in Compression. ACI J Proc 1985;82:797–804. https://doi.org/10.14359/10390.

[57] Wijesiri Pathirana S, Uy B, Mirza O, Zhu X. Flexural behaviour of composite steel–concrete beams utilising blind bolt shear connectors. Eng Struct 2016;114:181–94. https://doi.org/10.1016/j.engstruct.2016.01.057.

[58] Katwal U, Tao Z, Hassan MK, Uy B, Lam D. Load sharing mechanism between shear studs and profiled steel sheeting in push tests. J Constr Steel Res 2020;174:106279. https://doi.org/10.1016/j.jcsr.2020.106279.

[59] Guezouli S, Lachal A. Numerical analysis of frictional contact effects in push-out tests. Eng Struct 2012;40:39–50. https://doi.org/10.1016/j.engstruct.2012.02.025.

[60] Sjaarda M, Porter T, West JS, Walbridge S. Fatigue Behavior of Welded Shear Studs in Precast Composite Beams. J Bridg Eng 2017;22:04017089. https://doi.org/10.1061/(ASCE)BE.1943-5592.0001134.

[61] Liu X, Bradford MA, Chen Q-J, Ban H. Finite element modelling of steel–concrete composite beams with high-strength friction-grip bolt shear connectors. Finite Elem Anal Des 2016;108:54–65. https://doi.org/10.1016/j.finel.2015.09.004.

[62] Nguyen TNH, Tan KH, Kanda T. Investigations on web-shear behavior of deep precast, prestressed concrete hollow core slabs. Eng Struct 2019;183:579–93. https://doi.org/10.1016/j.engstruct.2018.12.052.

[63] Lawson RMM, Lim J, Hicks SJJ, Simms WII. Design of composite asymmetric cellular beams and beams with large web openings. J Constr Steel Res 2006;62:614–29. https://doi.org/10.1016/j.jcsr.2005.09.012.